Available online at www.sciencedirect.com
SCIENCE DIRECT®
Journal of Catalysis 222 (2004) 493–498
JOURNAL OF CATALYSIS
www.elsevier.com/locate/jcat

An efficient ruthenium catalyst for selective hydrogenation of *ortho*-chloronitrobenzene prepared via assembling ruthenium and tin oxide nanoparticles

Bojun Zuo,[b] Yuan Wang,[a,*] Qilong Wang,[b] Junling Zhang,[a] Nianzu Wu,[a] Lidan Peng,[a] Linlin Gui,[a] Xiaodong Wang,[a] Rongming Wang,[c] and Dapeng Yu[c]

[a] *State Key Laboratory for Structural Chemistry of Unstable and Stable Species, College of Chemistry and Molecular Engineering, Peking University, Beijing 100871, China*
[b] *Department of Chemistry, Shandong University, Jinan 250100, China*
[c] *Electron Microscopy Laboratory, School of Physics, Peking University, Beijing 100871, China*

Received 7 July 2003; revised 16 October 2003; accepted 1 December 2003

Abstract

A Ru/SnO_2 catalyst was prepared by capturing "unprotected" Ru nanoclusters on SnO_2 colloidal particles via electrostatic interaction followed by gelating the obtained complex sol by adjusting its pH value to 7. The assembled Ru/SnO_2 catalyst performed excellently in selectively hydrogenating *ortho*-chloronitrobenzene to the corresponding *o*-chloroaniline, the catalytic activity surpassing that of previously reported Ru catalysts and the selectivity for *ortho*-chloroaniline in agreement with the best results reported so far on a colloidal Ru catalyst. Obvious promotional effects of the SnO_2 support on both the catalytic activity and the selectivity were observed for the first time. A decrease of the reactivity of the C–Cl bond of *o*-chloroaniline over the present catalyst is one of the predominant reasons for the high selectivity at complete conversion. The catalyst structure was characterized by STEM, XPS, BET, and XRD.

Keywords: Ruthenium; Nanoparticles; Tin dioxide sol; Gel; Catalyst; Hydrogenation; *ortho*-Chloronitrobenzene

1. Introduction

Metal nanoclusters, as building blocks for preparing heterogeneous catalysts, offer new possibilities of universal significance for designing and constructing structure-controllable catalysts [1–19]. The support-entrapment method provides a realistic strategy, which builds a framework of inorganic supports around preformed metal nanoclusters [9–18]. In this method, to obtain a close contact of the metal nanoparticles with inorganic supports, organic stabilizers adsorbed on the preformed metal nanoclusters usually must be removed by extraction [11,12] or pyrolysis [14–18] at the end of the catalyst preparation. Recently, we have succeeded in effectively preparing a series of "unprotected" Pt, Rh, and Ru metal nanoclusters with small particle sizes and narrow size distributions that are stabilized by ethylene glycol and simple ions such as OH^- [20]. Herein we present a strategy, as illustrated in Scheme 1, to entrap our unprotected metal nanoclusters in gelated metal oxide nanoparticles, i.e., capturing the small metal nanoclusters on colloidal particles of metal oxides via electrostatic interaction and gelating the complex sol by adjusting its pH value. The assembly process using two kinds of nanoparticles stabilized with simple ions as building blocks adopted in this work is different from those based on an in situ hydration process of $M(OR)_n$ compounds in the presence of ligand-protected metal nanoclusters reported previously [11–18]. The so-prepared objective catalysts become more regulable in structure.

Hydrogenation of chloronitrobenzene (CNB) to the corresponding chloroaniline (CAN) (see Scheme 2 [21]) is of industrial interest and has been well studied over supported Pt and Pt-alloy catalysts for their high catalytic activities combined with a relatively low catalytic dehalogenation rate [22,23]. Tijani et al. [24] reported that Ru or its alloy catalysts supported on Al_2O_3 exhibited high

* Corresponding author.
E-mail address: wangy@pku.edu.cn (Y. Wang).

0021-9517/$ – see front matter
doi:10.1016/j.jcat.2003.12.007

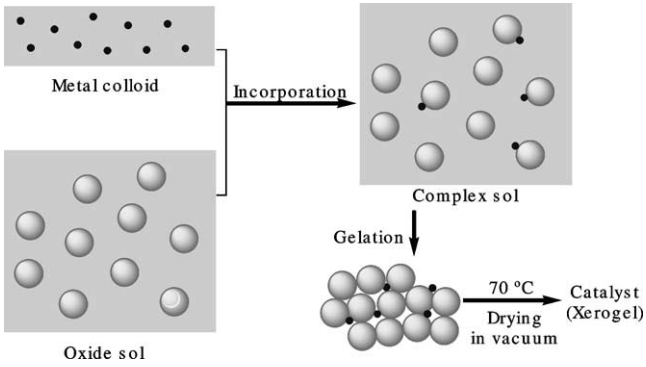

Scheme 1. General scheme showing the entrapment process of "unprotected" ruthenium nanoparticles within tin dioxide nanoparticles.

selectivity to CAN; however, conversions of CNB over these catalysts hardly reached 30%. Liu and co-workers recently revealed that metal ions such as Fe^{3+}, Co^{2+}, Sn^{2+}, or some boron species could improve both the catalytic activity and the selectivity of poly(*N*-vinyl-2-pyrrolidone) (PVP)-protected Ru colloid catalysts for the hydrogenation of CNB [25,26]. Encouraged by these achievements, we assembled a Ru/SnO_2 heterogeneous catalyst using the strategy depicted in Scheme 1 to explore the effects of species at the SnO_2 surface on the catalytic properties of Ru nanoparticles for the hydrogenation of *o*-CNB.

It was found that the catalytic activity for the selective hydrogenation of *o*-CNB to *o*-CAN over the assembled Ru/SnO_2 catalyst is much higher than that of other heterogeneous Ru catalysts or colloidal Ru catalysts reported previously. Coq and co-workers [23,24] have reported that modulating the interaction between metal particles and supports or the composition and size of the metal particles could improve the selectivity to *o*-CAN and that the reason for this behavior is not a decrease of the reactivity of the C–Cl bond of CAN over heterogeneous catalysts, but a lower adsorption strength of CAN with respect to CNB. In this work, however, an extremely low dehalogenation rate was observed over the present Ru/SnO_2 catalyst in the absence of CNB that should be responsible for the obtained high selectivity at complete conversion. The as-prepared Ru/SnO_2 catalyst also exhibits perfect stability.

2. Experimental

2.1. Materials and instruments

All reagents used in this work were analytical grade. Hydrogen with a purity of 99.999% was purchased from Beijing Gases Factory. TEM photographs were taken on a Philips Tecnai F30 scanning transmission electron microscope (STEM) equipped with a high-angle annular dark-field (HAADF) detector. The XPS measurement was conducted via an Axis Ultra photoelectron spectrometer.

2.2. Colloid fabrication

An ethylene glycol colloidal solution of Ru nanoparticles (3.7 g Ru/L) with an average diameter of 1.3 nm and a size distribution ranging from 0.9 to 2.2 nm was prepared according to the method reported previously [20]. The preparation of the SnO_2 sol was loosely based on a documented recipe [27]. An amount of 20 ml stannic chloride was dropped into 80 ml propanol and the mixture was cooled to ambient temperature. A solution of 10 ml distilled water in 40 ml propanol was then added to the mixture. The obtained mixture was stirred for 1 h, and then a solution of 20 ml distilled water in 80 ml of isopropanol was added. A SnO_2 sol was produced after further stirring the resulting colloidal solution for 1 h.

2.3. Catalyst preparation

The Ru/SnO_2 nanocomposite catalyst was prepared as follows: 5.4 ml of the prepared colloidal Ru solution was added to 99 ml of the prepared SnO_2 sol under stirring. After stirring for 20 min, the obtained complex sol was neutralized to pH 7 by adding an aqueous solution of sodium hydroxide (10 mol/L), resulting in gelation of the complex sol. The

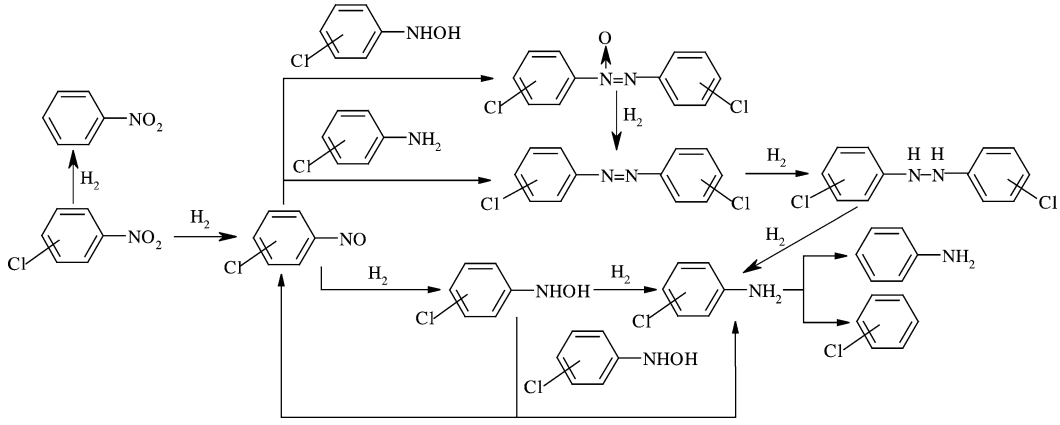

Scheme 2. The hydrogenation reaction pathways of chloronitrobenzene.

obtained precipitate was washed with water, separated by centrifugation, dried at 343 K in vacuum, and kept in a desiccator for use. The Ru content of the obtained catalyst was 0.9% as measured by means of ICP-AES.

A PVP-protected Ru colloid was prepared by mixing a glycol solution (5.0 ml) of PVP (206 mg, average molecular weight 58,000) with the colloidal solution of Ru (3.7 mg in 1.0 ml glycol) under stirring. For use as a catalyst, the PVP–Ru nanoclusters were separated as a precipitate from the colloidal solution by adding acetone and then "dissolved" in 25 ml methanol.

A classical Pt/SnO_2 heterogeneous catalyst (Ru/SnO_2-imp) with 1% Pt loading was also prepared by the traditional wetness impregnation method using $H_2PtCl_6 \cdot 6H_2O$ and a prepared SnO_2 support as the precursors. The SnO_2 support was prepared by neutralizing the prepared SnO_2 sol with an aqueous solution of NaOH and drying the SnO_2 precipitate at 393 K. The catalyst was calcined at 573 K for 2 h and reduced with hydrogen at 523 K for 3 h.

2.4. Catalytic hydrogenation of CNB

Hydrogenation of CNB was performed at 333 K and 4.0 MPa of hydrogen pressure in a 100-ml stainless-steel autoclave. Typically, the autoclave was charged with 0.1 g nanocomposite Ru/SnO_2 catalyst, 1.2 mmol *o*-CNB, 0.2 g dodecanol (as GC internal standard), and 25 ml methanol. Air in the system was removed by sweeping the system three times with hydrogen. The reaction mixture was stirred for a certain time at 333 K. Hydrogenation products were analyzed on a Beifen 3420 gas chromatograph equipped with a FID detector and a DC-710 packed column.

3. Results and discussion

3.1. Characterization of the assembled catalyst

For preparing the Ru/SnO_2 catalyst, an ethylene glycol colloidal solution of our unprotected Ru nanoclusters with an average particle size of 1.3 nm was incorporated in a tin dioxide sol (see the Experimental Section), resulting in a transparent colloidal solution without any precipitate. We have reported that a Ru precipitate will appear when the Ru colloidal solution comes into contact with an aqueous acidic solution [20]. Therefore, we believe that in the mixed sol Ru nanoparticles are adsorbed on the SnO_2 colloidal particles via electrostatic interaction between the nanoparticles, which was clearly confirmed by Z-contrast images of the Ru/SnO_2 complex nanoparticles as shown in Fig. 1a.

In Fig. 1a, it is easy to discern the spots with different brightness that reflect an ability of elastically scattering electrons. A combined EDX analysis, using an electron beam of 0.8 nm in diameter, showed that the signal of ruthenium could be detected only at the small brightest spots, while that of tin was widely present in the bright area in Fig. 1a. Therefore, we conclude that the brightest cores in the bright area are the images of Ru nanoclusters. The particle sizes of the Ru nanoclusters, measured from the Z-contrast images, range from 1 to 2.5 nm. Considering the relative low space resolution of Z-contrast images, this result agrees well with that of the original Ru nanoclusters in colloidal solution, suggesting that the Ru nanoparticles are entrapped in the matrix of the SnO_2 support without obvious aggregation.

The X-ray diffraction pattern (Fig. 2) of the Ru/SnO_2 catalyst containing 0.9% Ru revealed that tin dioxide cassiterite was formed with an average crystal grain size of 7.6 nm, in good agreement with the results of the HRTEM measurements shown in Fig. 1b. Diffraction signals of the Ru nanoparticles cannot be observed in the XRD pattern due to the low concentration and small particle size of the Ru nanoclusters.

The binding energy of the Ru $3d_{5/2}$ level in the Ru/SnO_2 catalyst, measured from its XPS spectrum, had a value of 280.1 eV, revealing that Ru nanoparticles in the assembled catalyst were in the metallic state.

The N_2 adsorption–desorption isotherm of the Ru/SnO_2 nanocomposite catalyst is of type I, revealing a microporous structure of the catalyst. The BET surface area was 146.4 m^2/g and the pore volume was 0.093 cm^3/g. The Horvath–Kawazoe pore diameter was 1.2 nm.

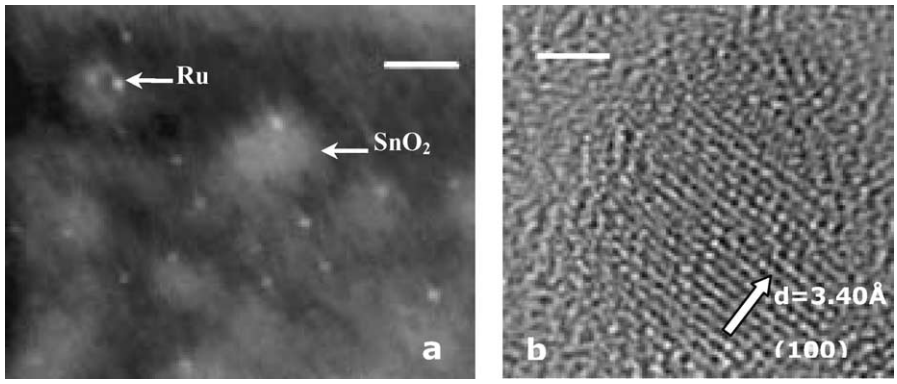

Fig. 1. (a) HAADF STEM images showing Ru nanoparticles captured on the surface of tin dioxide particles, the bar equals 20 nm; (b) HRTEM image of a tin dioxide nanocrystal grain characterized by interplanar distances of 3.40 Å of cassiterite (100), the bar equals 2 nm.

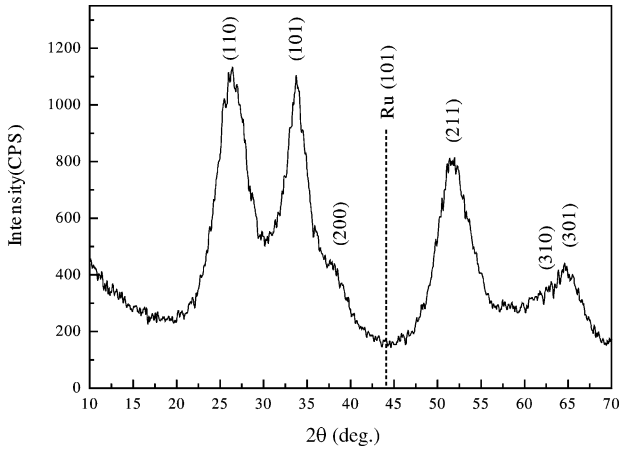

Fig. 2. XRD pattern of the ruthenium-entrapped tin dioxide (Ru/SnO_2) catalyst.

3.2. Catalytic properties for the selective hydrogenation of *o*-CNB

The catalytic properties of the Ru/SnO_2, PVP–Ru, and Ru/SnO_2-imp catalysts for the selective hydrogenation of *o*-CNB to *o*-CAN are reported in Table 1. An *o*-CAN selectivity over 99.9% at a substrate conversion of 100% was obtained over the Ru/SnO_2 nanocomposite catalyst. This selectivity is comparable to the best results reported for a modified PVP–Ru colloidal catalyst [25,26], and is better than that of the PVP–Ru colloidal catalyst which has the same Ru nanoparticles (prepared in this work; see the Experimental Section). It is known that for the catalytic reaction of interest, a high selectivity is difficult to maintain once the substrate has been exhausted completely over most metal-supported catalysts since in the absence of substrate, the catalytic dehalogenation reaction will occur at a much faster rate. To our surprise, it was observed that the dehalogenation rate of *o*-CAN over the present Ru/SnO_2 catalyst was as low as 1.55×10^{-4} mol-*o*-CAN/(mol-Rus) in the absence of *o*-CNB, whereas the dehalogenation rate over the PVP–Ru colloidal catalyst has a value of 3.44×10^{-3} mol-*o*-CAN/(mol-Rus). Therefore, the observed outstanding selectivity at complete conversion of *o*-CNB over the Ru/SnO_2 catalyst is not only due to a relatively strong adsorption ability of *o*-CNB on the catalyst as observed on other metal catalysts, but also to a remarkable decrease in the dehalogenation rate.

Table 1
Catalytic properties of different catalysts

	Catalyst			
	Ru/SnO_2	Ru–PVP[b]	Ru–PVP[c]	Ru/SnO_2-imp[d]
	Selective hydrogenation of *o*-CNB			
o-CAN selectivity (%)	> 99.9	99.9	> 99.9	> 99.9
Reaction rate[a]	4.3×10^{-2}	6.9×10^{-3}	5.0×10^{-3}	5.9×10^{-4}
Conversion of (%) *o*-CNB	100	99	100	20
	Dehalogenation of *o*-CAN			
Dehalogenation rate[a]	1.55×10^{-4}	3.44×10^{-3}		

All reactions were conducted at 333 K and 4.0 MPa of H_2 pressure.

[a] Reaction rate unit: mol-substrates/(mol-Ru s).

[b] PVP–Ru colloidal catalyst prepared in this work.

[c] Data from the literature [24]; reaction was conducted at 320 K and 4.0 MPa of H_2 pressure over a boride-modified PVP–Ru colloidal catalyst.

[d] A 0.2 g Ru/SnO_2-imp catalyst was charged into the reactor with 1.2 mmol substrate and 20 ml methanol.

The catalytic activity over the present Ru/SnO_2 nanocomposite catalyst is 8 times higher than that of the boride-modified PVP–Ru colloid catalyst reported by Liu et al. [25], and 6 times higher than that of the PVP–Ru nanoclusters having the same Ru metal nanoparticles prepared in this work, suggesting that SnO_2 nanoparticles in the nanocomposite catalyst have a promotion effect on the catalytic activity of the Ru nanoparticles. Moreover, the catalytic activity of the Ru/SnO_2-imp catalyst prepared by the traditional impregnation method was much lower than that of the Ru/SnO_2 nanocomposite catalyst.

The stability of the Ru/SnO_2 catalyst is also perfect. After reusing it three times, the recovered catalyst maintained its catalytic activity completely. In a series of experiments, the catalytic activity for the new catalyst was 4.27×10^{-2} mol-substrates/(mol-Rus), and those for the three times recovered catalysts were 4.30×10^{-2}, 4.33×10^{-2}, and 4.25×10^{-2} mol-substrates/(mol-Rus), respectively. The selectivity for *o*-CAN stayed over 99.8% after a turnover number of 3×10^4 mol-*o*-CNB/mol-Ru was achieved.

Coq et al. compared the catalytic properties for the hydrogenation of *p*-CNB over Pt/TiO_2 and Pt/Al_2O_3 catalysts prepared by classical methods [23], and proposed that suboxide TiO_x species migrating on the Pt particles could polarize the N=O bond in *p*-CNB and were responsible for promoting the Pt properties for the selective hydrogenation of *p*-CNB to *p*-CAN. It was reported that the ratio of the hydrogenation activity to hydrodechlorination activity over the Pt/TiO_2 catalyst (SMSI state) was 10-fold higher than that over the Pt/Al_2O_3 catalyst. It should be noted that the absolute catalytic activity for the hydrodechlorination over Pt/TiO_2 is also two times higher than that of the Pt/Al_2O_3 catalyst, i.e., the suboxide TiO_x species accelerate not only the hydrogenation of *p*-CNB but also the hydrodechlorination of *p*-CAN in the absence of *p*-CNB. In the present Ru/SnO_2 nanocomposite catalyst, however, the catalytic activity of the Ru nanoparticles for the hydrogenation of *o*-CNB was remarkably promoted, while that for the hydrodechlorination was distinctly depressed.

SnO_2 is widely applied in the fabrication of chemical sensors for the detection of reductive gases [28], whereas it is seldom used as a support for hydrogenation catalysts. The concentration of oxygen vacancies or coordinatively unsaturated Sn^{4+} or Sn^{2+} species at the surface of SnO_2 will increase when the material is treated in reducing atmospheres such as H_2 or CO [28]. These surface species, that in the present catalyst surround the Ru metal nanoclus-

ters, may activate the polar NO_2 groups of *o*-CNB and coordinate with the NH_2 groups of produced *o*-CAN molecules, thereby promoting the hydrogenation of *o*-CNB and depressing the dehalogenation of *o*-CAN in a manner similar to, but more effectively than, that of metal cations in the colloidal solution of PVP–Ru catalysts [25,26]. It is interesting to note that Sn^{2+} added as $SnCl_2$ in the PVP-protected Ru colloid catalytic system has only a weak promotion effect on the catalytic activity [25] (increasing the rate by 18%), while the catalytic activity of our Ru/SnO_2 catalyst is six times higher than the PVP–Ru nanocluster catalyst having the same Ru particles.The difference in the promotion effects between the surface-fixed modifiers and those of metal cations such as Sn^{2+} in solution should not only be derived from their chemical structures but also from their mobility. In a colloidal metal solution, metal cations may adsorb on the negatively charged metal particles. An adsorption–desorption equilibrium will occur before a whole layer of metal cations surrounding the metal nanoparticles appears because of the repulsion between the cations. On the other hand, the counterions such as Cl^- are competing with the NH_2 groups in *o*-CAN for coordinating positions of metal cations. Both drawbacks will weaken the promotion effect of Sn^{2+} and can be avoided over our Ru/SnO_2 nanocomposite catalyst. This accounts for its extremely high catalytic activity for the hydrogenation of *o*-CNB compared with other reported Ru catalysts and low dehalogenation rate for produced *o*-CAN.

To confirm the specific effect of the SnO_2 nanoparticles in the Ru/SnO_2 catalyst on depressing the hydrodechlorination of *o*-CAN, we prepared a Ru/SiO_2 catalyst using the process depictured in Scheme 1. In the absence of *o*-CNB, the hydrodechlorination rate over the Ru/SiO_2 nanocomposite catalyst, under the same reaction conditions shown in Table 1, was 1.13×10^{-2} mol-*o*-CAN/(mol-Rus), which was 73 times higher than that over the Ru/SnO_2 nanocomposite catalyst. The selectivity of *o*-CAN over this Ru/SiO_2 catalyst was 95% at complete *o*-CNB conversion.

4. Conclusion

In this paper, we describe a novel Ru/SnO_2 nanocomposite catalyst prepared by expediently stacking nanoparticles of SnO_2 around unprotected small Ru nanoparticles with an average particle size of 1.3 nm. The specific surface area and the average pore size of the catalyst are 146.4 m^2/g and 1.2 nm, respectively. The prepared Ru/SnO_2 nanocomposite catalyst displays excellent catalytic properties for the hydrogenation of *o*-chloronitrobenzene to corresponding chloroaniline. The catalytic activity for the reaction of interest over the present Ru/SnO_2 nanocomposite catalyst is six times higher than the PVP–Ru nanoclusters having the same Ru metal nanoparticles and is much higher than the most effective Ru metal catalyst reported previously. A remarkable promotion effect of SnO_2 on the catalytic activity of Ru nanoparticles and an extremely low dehalogenation rate of *o*-CAN over the Ru/SnO_2 catalyst were observed for the first time, which may partly be derived from the coordination action between the NH_2 groups in *o*-CAN and coordinatively unsaturated Sn^{4+} or Sn^{2+} species at the surface of SnO_2, revealing a realistic way for further improving the catalytic activity of the highly selective Ru metal catalyst for the hydrogenation of CNB by alternating the composition and structure of the metal–semiconductor nanocomposite catalysts. Studies on the details of the catalytic mechanism of the promising Ru/SnO_2 catalyst and the catalytic properties of other assembled nanocomposite catalysts prepared via the strategy proposed in this work are being continued.

Acknowledgments

This work was financially supported by the Major State Basic Research Development Program (Project No. G2000077503) from the Chinese Ministry of Science and Technology and grants from NSFC (Project No. 29925308, 90206011).

References

[1] J. Turkevich, G. Kim, Science 169 (1970) 873.
[2] D.N. Furlong, D. Wells, W.H.F. Sasse, J. Phys. Chem. 89 (1985) 626.
[3] Y. Wang, H.F. Liu, Y.Y. Jiang, J. Chem. Soc. Chem. Commun. 1878 (1989).
[4] Y. Wang, H.F. Liu, Y. Huang, Polym. Adv. Technol. 7 (1996) 634.
[5] U. Junges, F. Schöth, G. Schmid, Y. Uchida, R. Schlögl, Ber. Bunsen-Ges. 101 (1997) 1631.
[6] A. Martino, S.A. Yamanaka, J.S. Kawola, D.A. Loy, Chem. Mater. 9 (1997) 423.
[7] W.Y. Yu, H.F. Liu, X.H. An, Z.J. Liu, X.M. Ma, J. Mol. Catal. A: Chem. 142 (1999) 201.
[8] N. Toshima, Y. Shiraishi, T. Teranishi, M. Miyake, T. Tominaga, H. Watanabe, W. Brijoux, H. Bönnemann, G. Schmid, Appl. Organomet. Chem. 15 (2001) 178.
[9] M. Kishida, K. Ichiki, T. Hanaoka, H. Nagata, K. Wakabayashi, Catal. Today 45 (1989) 203.
[10] C. Lange, D. De Caro, A. Gamez, S. Storck, J.S. Bradley, W.F. Maier, Langmuir 15 (1999) 5333.
[11] M.T. Reetz, M. Dugal, Catal. Lett. 58 (1999) 207.
[12] A. Martino, A.G. Sault, J.S. Kawola, E. Boespflug, M.L.F. Phillips, J. Catal. 187 (1999) 30.
[13] A.G. Sault, A. Martino, J.S. Kawola, E. Boespflug, J. Catal. 191 (2000) 474.
[14] H. Bönnemann, U. Endruschat, B. Tesche, A. Rufínska, C.W. Lehmann, F.E. Wagner, G. Filoti, V. Pârvulescu, V.I. Pârvulescu, Eur. J. Inorg. Chem. 5 (2000) 819.
[15] J.P.M. Niederer, A.B.J. Arnold, W.F. Hölderich, B. Spliethof, B. Tesche, M.T. Reetz, H. Bönnemann, Top. Catal. 18 (2002) 265.
[16] Z. Kónya, V.F. Puntes, I. Kiricsi, J. Zhu, P. Alivisatos, G.A. Somorjai, Catal. Lett. 81 (2002) 137.
[17] Z. Kónya, V.F. Puntes, I. Kiricsi, J. Zhu, J.W. Ager, M.K. Ko, H. Frei, A.P. Alivisatos, G.A. Somorjai, Chem. Mater. 15 (2003) 1242.
[18] J. Zhu, Z. Kónya, V.F. Puntes, I. Kiricsi, C.X. Miao, J.W. Ager, A.P. Alivisatos, G.A. Somorjai, Langmuir 19 (2003) 4396.
[19] T. Yonezawa, H. Matsune, N. Kimizuka, Adv. Mater. 15 (2003) 499.

[20] Y. Wang, J. Ren, K. Deng, L. Gui, Y. Tang, Chem. Mater. 12 (2000) 1622.
[21] W. Pascoe, in: P.N. Rylander, H. Greenfield, R.L. Augustine (Eds.), Catalysis of Organic Reactions, Dekker, New York, 1988, p. 121.
[22] B. Coq, A. Tijani, F. Figueras, J. Mol. Catal. 71 (1992) 317.
[23] B. Coq, A. Tijani, R. Dutartre, F. Figueras, J. Mol. Catal. 79 (1993) 253.
[24] A. Tijani, B. Coq, F. Figueras, Appl. Catal. 76 (1991) 255.
[25] M.H. Liu, W.Y. Yu, H.F. Liu, J. Mol. Catal. A: Chem. 138 (1999) 295.
[26] X. Yan, M.H. Liu, H.F. Liu, K.Y. Liew, J. Mol. Catal. A: Chem. 16 (2001) 225.
[27] P. Siciliano, Sens. Actuators B 70 (2000) 153.
[28] D. Amalric-Popescu, F. Bozon-Verduraz, Catal. Today 70 (2001) 139.